

Supplementary Materials for
**Pulmonary neuroendocrine cell–derived exosomes regulate iron homeostasis
and oxidative stress in lung neurons**

Abhimanyu Thakur *et al.*

Corresponding author: Abhimanyu Thakur, abhimanyu@uchicago.edu;
Huanhuan Joyce Chen, joycechen@uchicago.edu

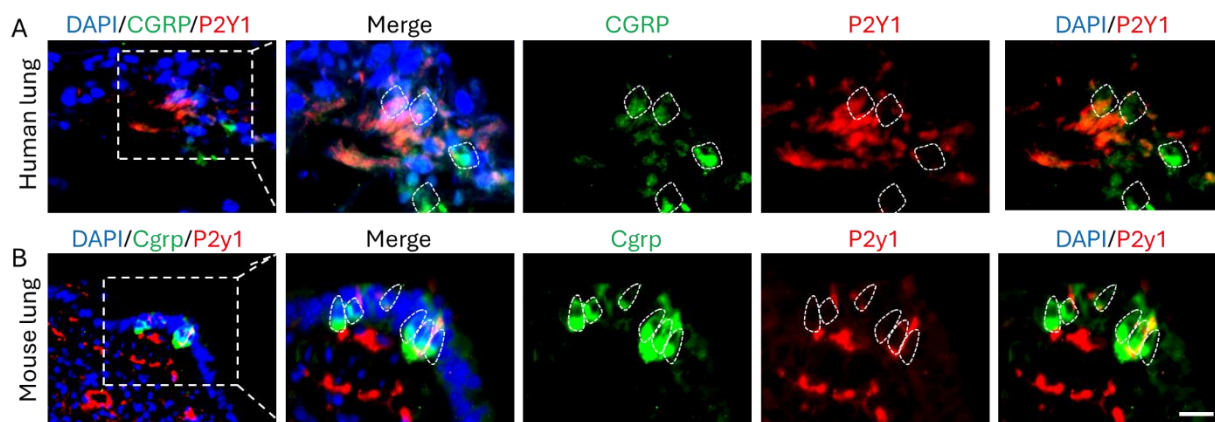
Sci. Adv. **12**, eady2696 (2026)
DOI: 10.1126/sciadv.ady2696

The PDF file includes:

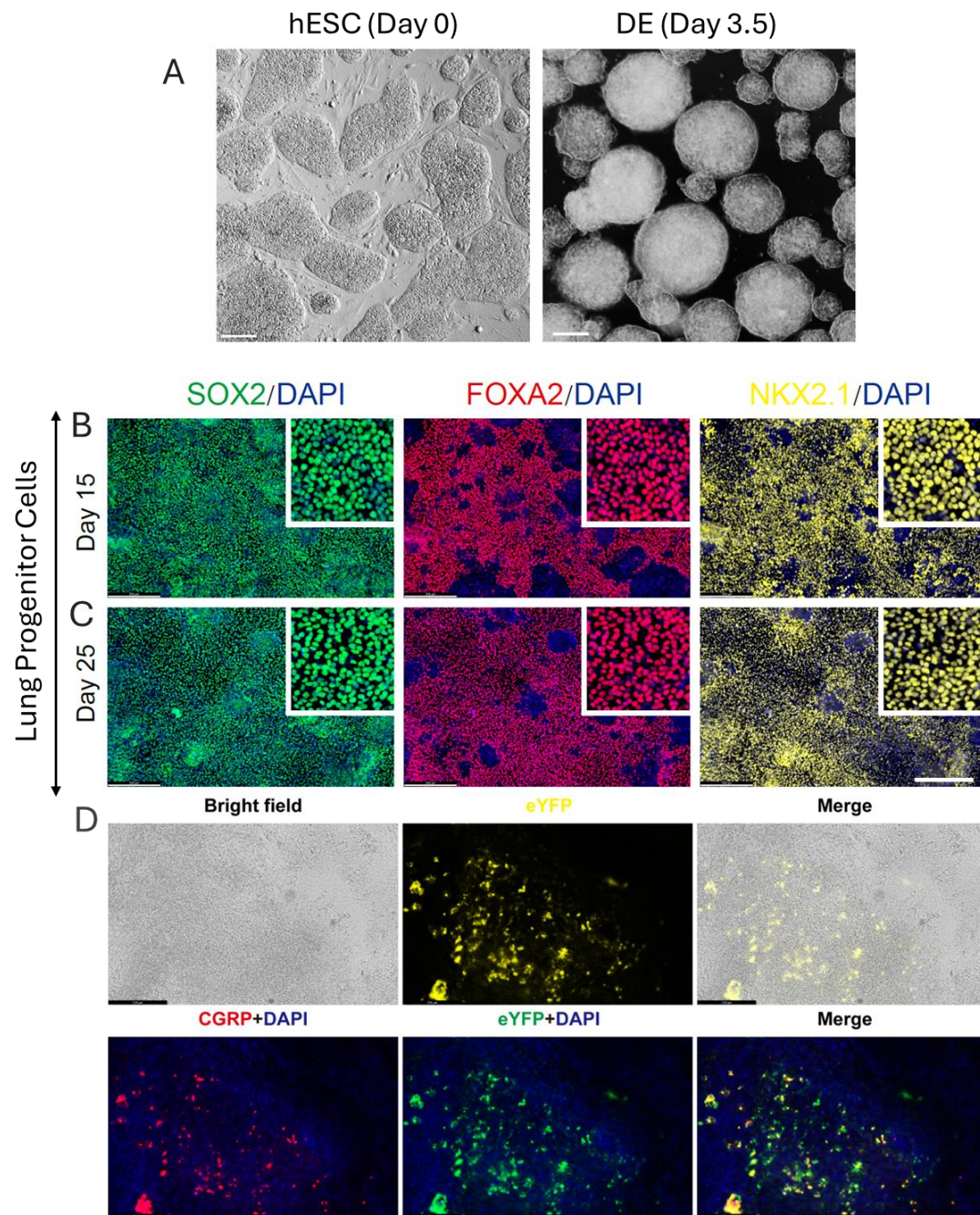
Figs. S1 to S27
Table S2
Legend for table S1
Legend for movie S1

Other Supplementary Material for this manuscript includes the following:

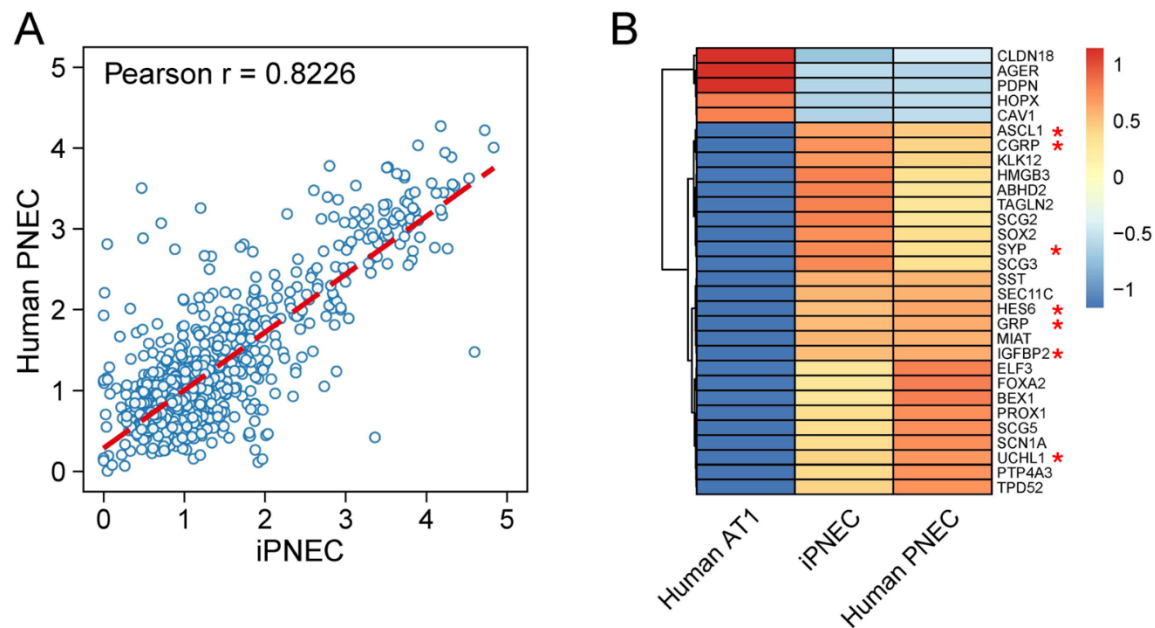
Table S1
Movie S1



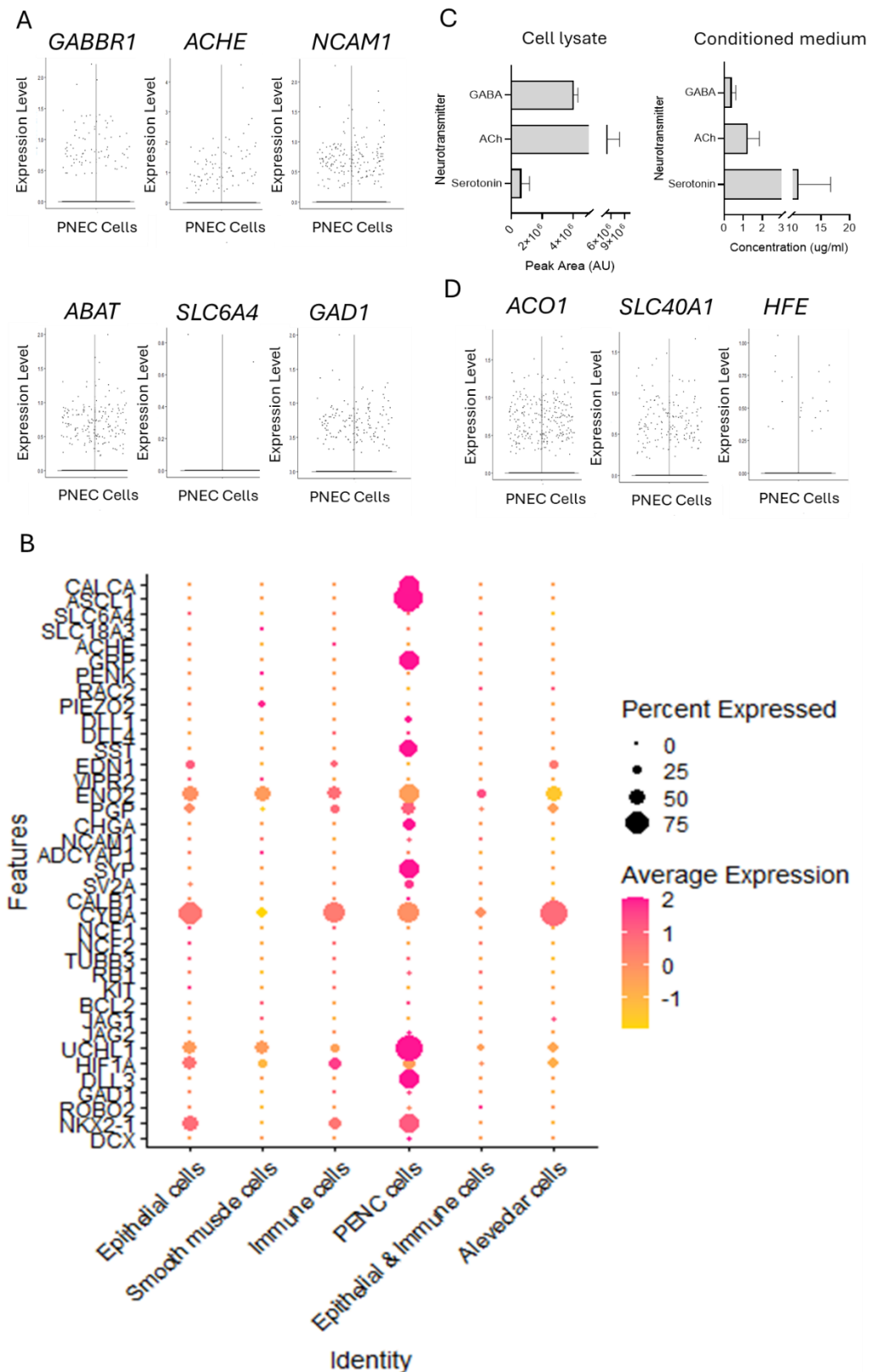
Supplementary Fig. S1. Analysis of neuro-innervation of PNEC in human and mouse lungs. (A, B) Representative immunofluorescence staining showing the co-localization of CGRP (for PNEC) and P2Y1 (a vagus marker) in the lung tissue of (A) human and (B) mouse. (Scale bar: 20 μ m).



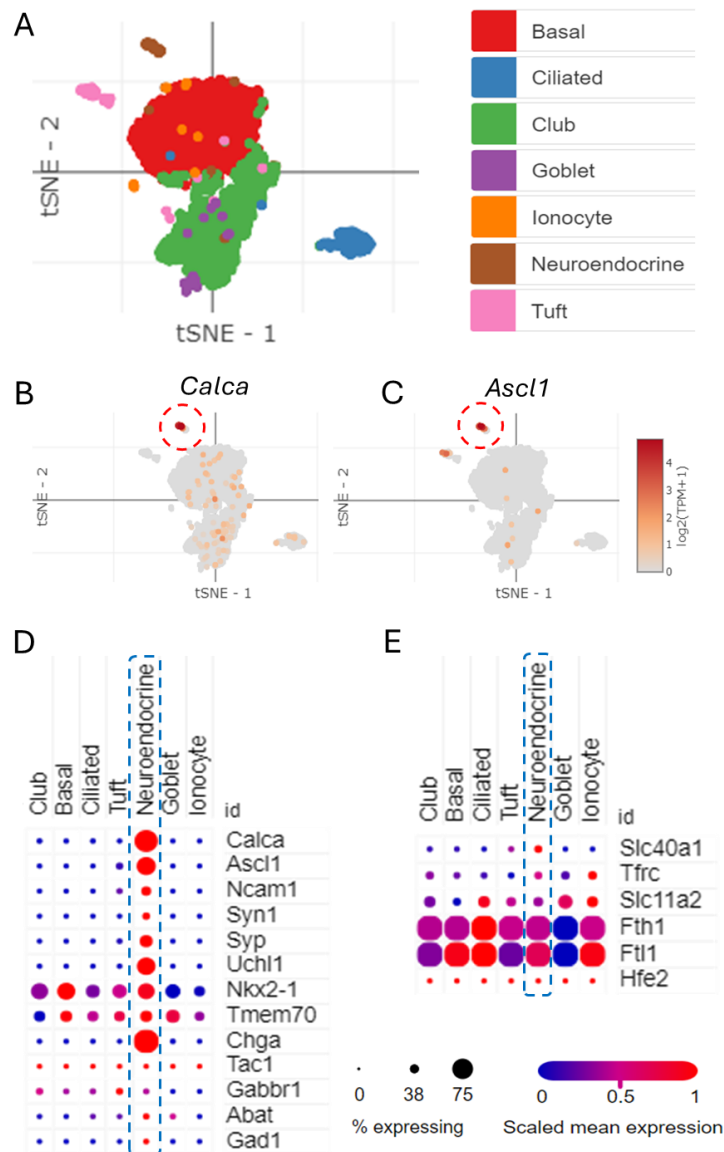
Supplementary Fig. S2. Differentiation of hESCs to produce definite endoderm (DE) and lung cells (LCs), and their characterization. (A) RUES2 cells were induced to produce DE. (B, C) Endoderm was differentiated to form LP cells between day 15 (B) and day 25 (C) as shown by increasing proportions of cells positive for NKX2.1, SOX2, and FOXA2. Day 25 LP cells derived from hESCs (RUES2 line) were further differentiated into cells resembling major types of LCs, including PNEC, as detected by immunofluorescence staining and flow cytometry analysis of CGRP+ cells (refer to main text Figure 2B-E). Scale bar = 200 μ m. (D) Brightfield and immunofluorescence images showing the expression of reporter gene, eYFP (shown as pseudo-green colour in lower panel) colocalized with CGRP (red colour) stained PNECs.



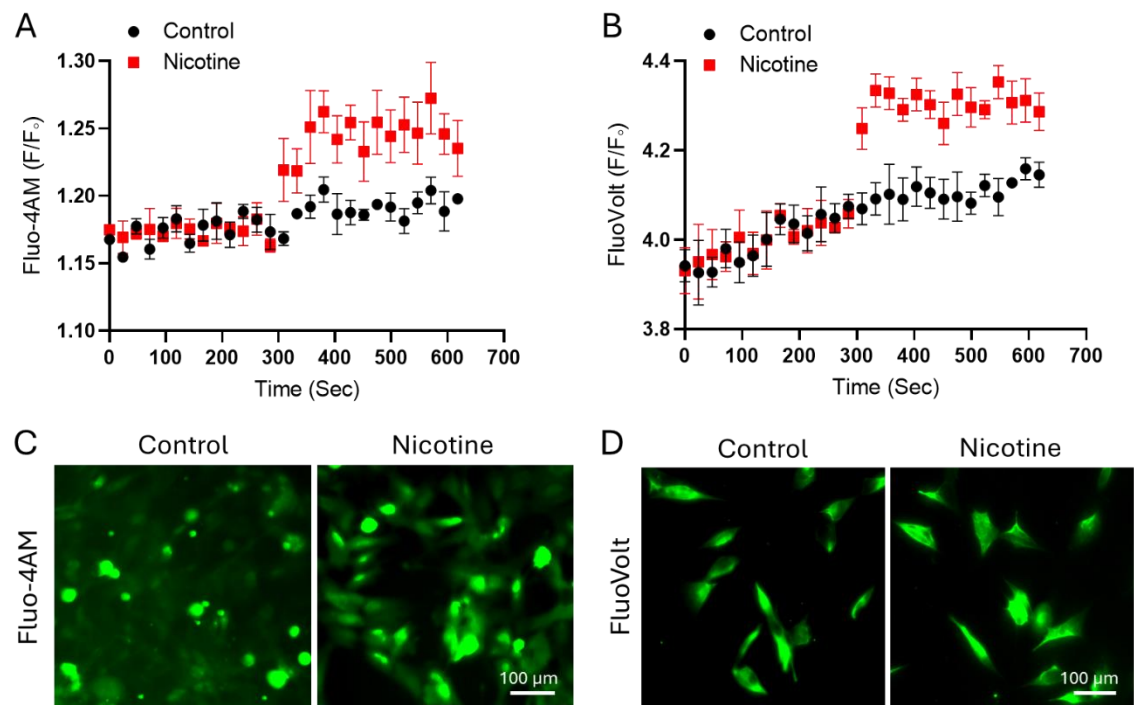
Supplementary Fig. S3. Determination of genetic profile similarity between iPNEC and human PNEC. Representative (A) correlation plot depicting the transcriptomic profile similarity of genes between the iPNEC and human PNEC, and (B) heatmap of selected PNEC markers (designed by asterisk).



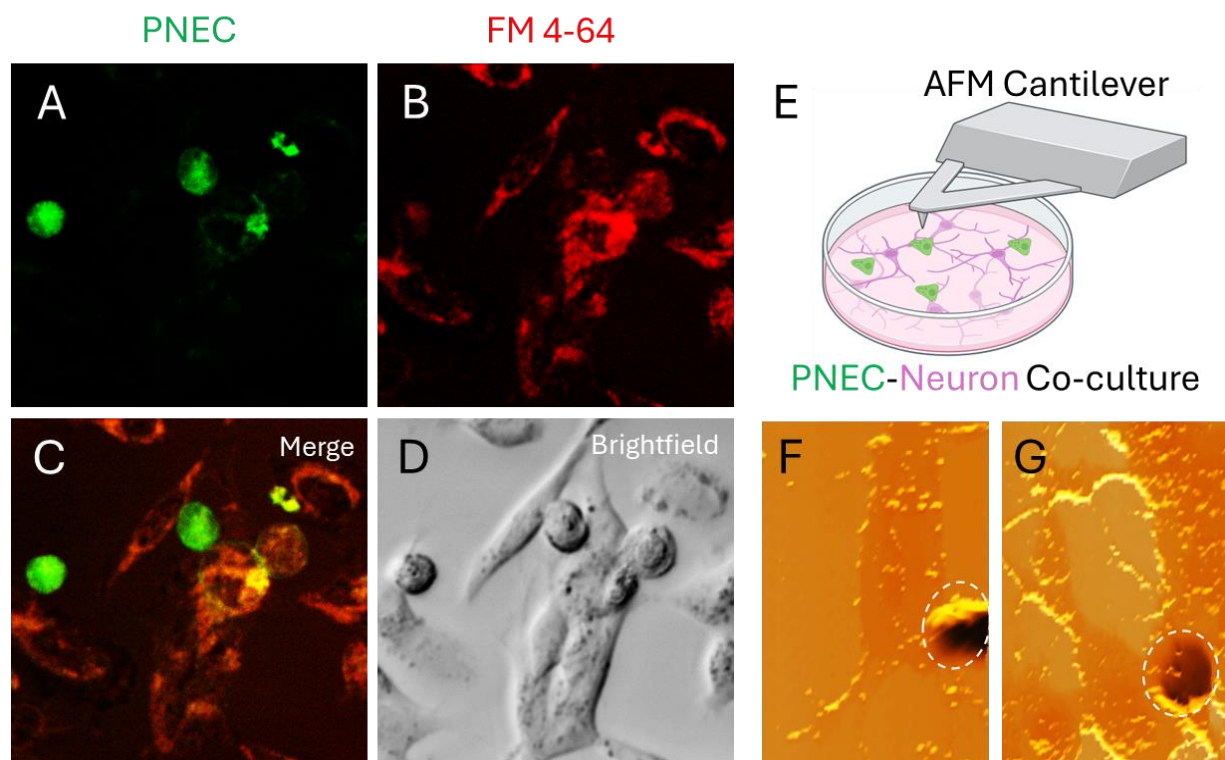
Supplementary Fig. S4. Characterization of iPNEC by scRNA-seq analysis. (A) Representative violin plots showing the expression of native human PNEC markers in the iPNEC. (B) Representative dot plot showing the cell type specific expression of major native human PNEC markers in hPSC-derived lung cell population. (C) Metabolomic analysis identified various neurotransmitters in the iPNEC lysate, which was further validated in conditioned medium of iPNEC via SPR analysis (N=2 replicates). (D) Representative violin plots showing the expression of major gene involved in the iron regulation, in the iPNEC. Figures are generated using our scRNA-seq data of iLung (batch 1 and 2).



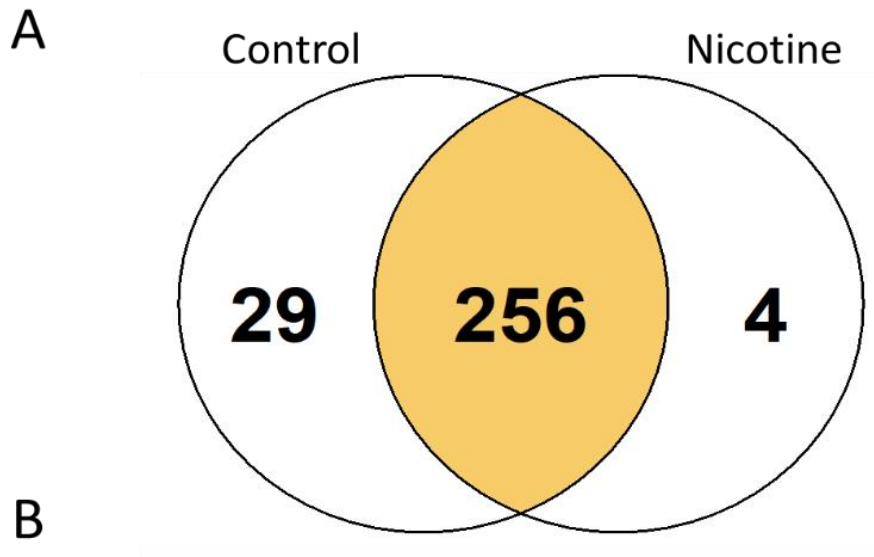
Supplementary Fig. S5. Validation of the presence of iron regulating markers in mouse PNEC. (A) tSNE map showing the clustering of different cell type sub-population at single cell level (GEO: GSE103354). (B, C) tSNE maps depicting the expression and distribution of (B) *Calca* and (C) *Ascl1* with major enrichment in PNEC cell type population. (D, E) Dot plots showing the cell type-specific expression of (D) major genes as biomarkers of PNEC and (E) genes involved in the iron regulation signaling. These figures are based on the public data (GEO: GSE103354) using Single Cell Portal of the Broad Institute.



Supplementary Fig. S6. Temporal effect of nicotine treated- iPNEC-derived exosomes on the neuronal cells. Representative graphs and fluorescence images depicting time-dependent (**A**, **C**) Fluo-4AM labelled intracellular calcium level and (**B**, **D**) FluoVolt labelled membrane potential of neuronal cells treated with control- and nicotine treated- iPNEC-derived exosomes, detected by plate reader-based Fura-4AM and FluoVolt signal recording.



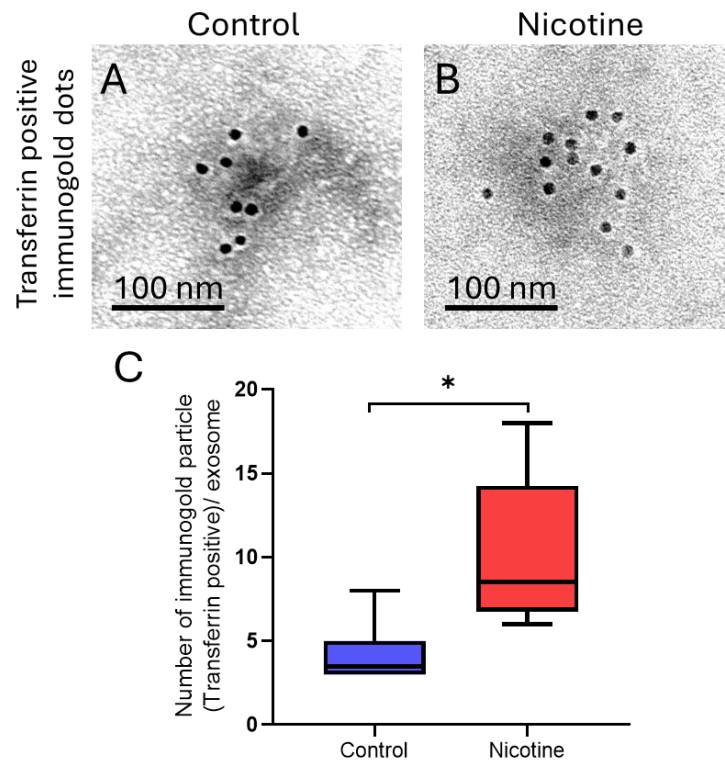
Supplementary Fig. S7. PNEC and neuronal cells interact in co-culture. (A-D) Representative (A-C) immunofluorescence (FM 4-64)- and (D) brightfield- image showed interaction between PNEC and HD10.6 neuronal cells. (E-G) AFM cantilever-based topographic images of interaction between PNEC and neuronal cells (views from two different regions). PNEC is an encircled one, which interacts with neuronal cells.



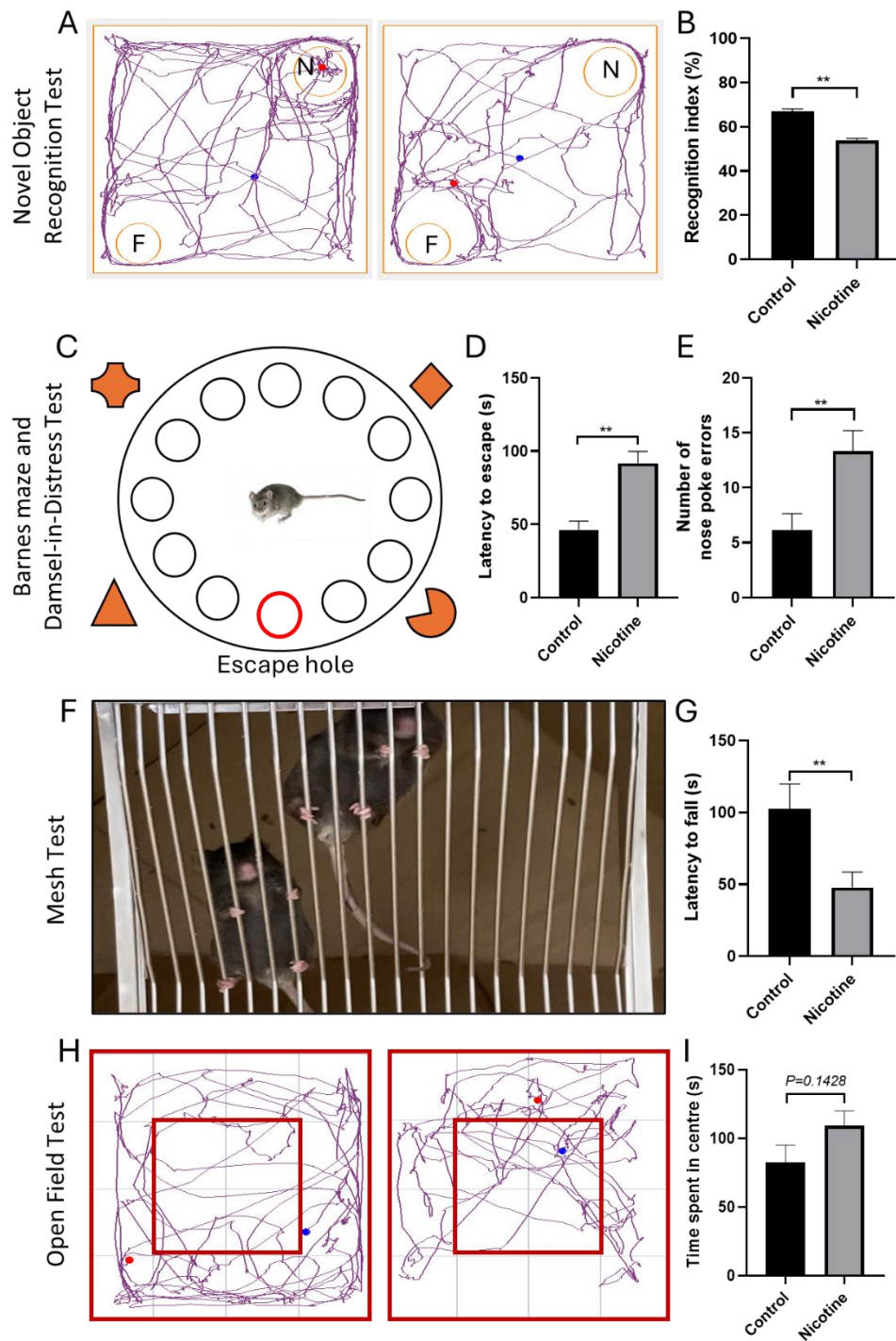
B

Accession	Protein Name
P02768	Serum albumin OS=Homo sapiens OX=9606 GN=ALB PE=1 SV=2
P02787	Serotransferrin OS=Homo sapiens OX=9606 GN=TF PE=1 SV=3
P06733	Alpha-enolase OS=Homo sapiens OX=9606 GN=ENO1 PE=1 SV=2
P04264	Keratin, type II cytoskeletal 1 OS=Homo sapiens OX=9606 GN=KRT1 PE=1 SV=6
P63261	Actin, cytoplasmic 2 OS=Homo sapiens OX=9606 GN=ACTG1 PE=1 SV=1
P13645	Keratin, type I cytoskeletal 10 OS=Homo sapiens OX=9606 GN=KRT10 PE=1 SV=6
P07437	Tubulin beta chain OS=Homo sapiens OX=9606 GN=TUBB PE=1 SV=2
P68363	Tubulin alpha-1B chain OS=Homo sapiens OX=9606 GN=TUBA1B PE=1 SV=1
Q71U36	Tubulin alpha-1A chain OS=Homo sapiens OX=9606 GN=TUBA1A PE=1 SV=1
P14618	Pyruvate kinase PKM OS=Homo sapiens OX=9606 GN=PKM PE=1 SV=4
P04406	Glyceraldehyde-3-phosphate dehydrogenase OS=Homo sapiens OX=9606 GN=GAPDH PE=1 SV=3
P35527	Keratin, type I cytoskeletal 9 OS=Homo sapiens OX=9606 GN=KRT9 PE=1 SV=3
P10809	60 kDa heat shock protein, mitochondrial OS=Homo sapiens OX=9606 GN=HSPD1 PE=1 SV=2
P13639	Elongation factor 2 OS=Homo sapiens OX=9606 GN=EEF2 PE=1 SV=4
P05787	Keratin, type II cytoskeletal 8 OS=Homo sapiens OX=9606 GN=KRT8 PE=1 SV=7
P06576	ATP synthase subunit beta, mitochondrial OS=Homo sapiens OX=9606 GN=ATP5F1B PE=1 SV=3
P35908	Keratin, type II cytoskeletal 2 epidermal OS=Homo sapiens OX=9606 GN=KRT2 PE=1 SV=2
P68104	Elongation factor 1-alpha 1 OS=Homo sapiens OX=9606 GN=EEF1A1 PE=1 SV=1
P35579	Myosin-9 OS=Homo sapiens OX=9606 GN=MYH9 PE=1 SV=4
P11021	Endoplasmic reticulum chaperone BiP OS=Homo sapiens OX=9606 GN=HSPA5 PE=1 SV=2

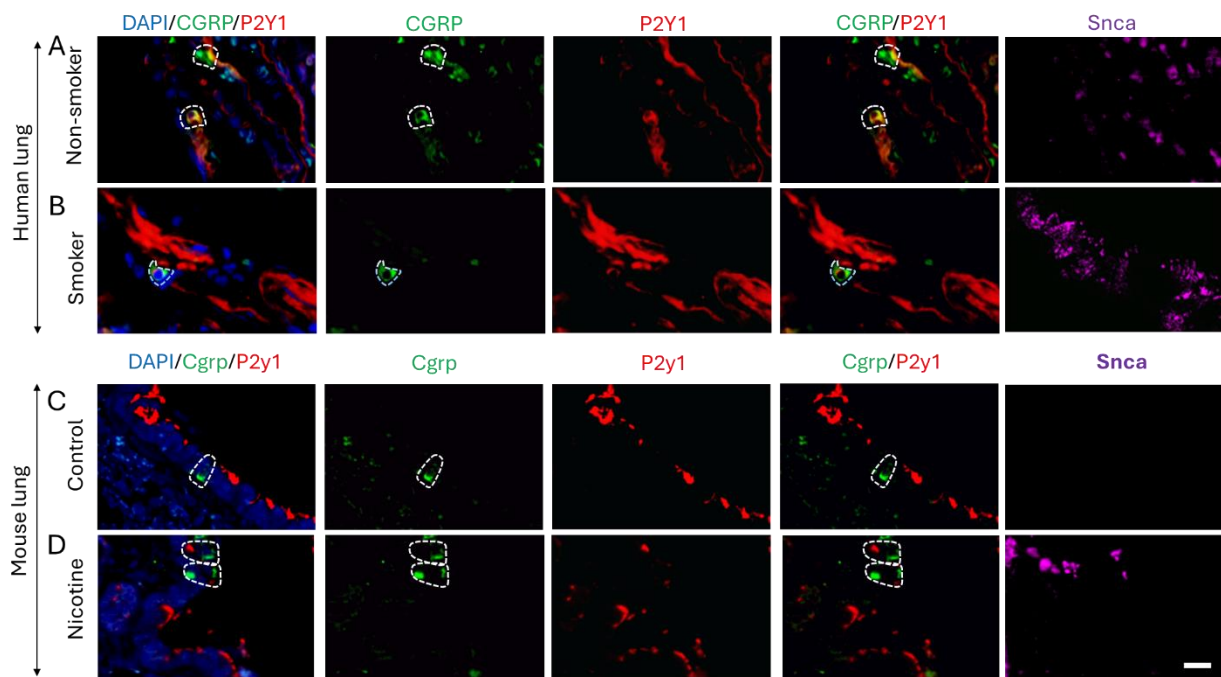
Supplementary Fig. S8. Proteomic analysis of control- and nicotine treated- iPNECs. (A) A typical Venn diagram showing the number of proteins present exclusive in either control- or nicotine treated- iPNECs, or common to both. **(B)** A list of protein with the corresponding accession number, significantly increased in nicotine treated iPNECs compared to the control group.



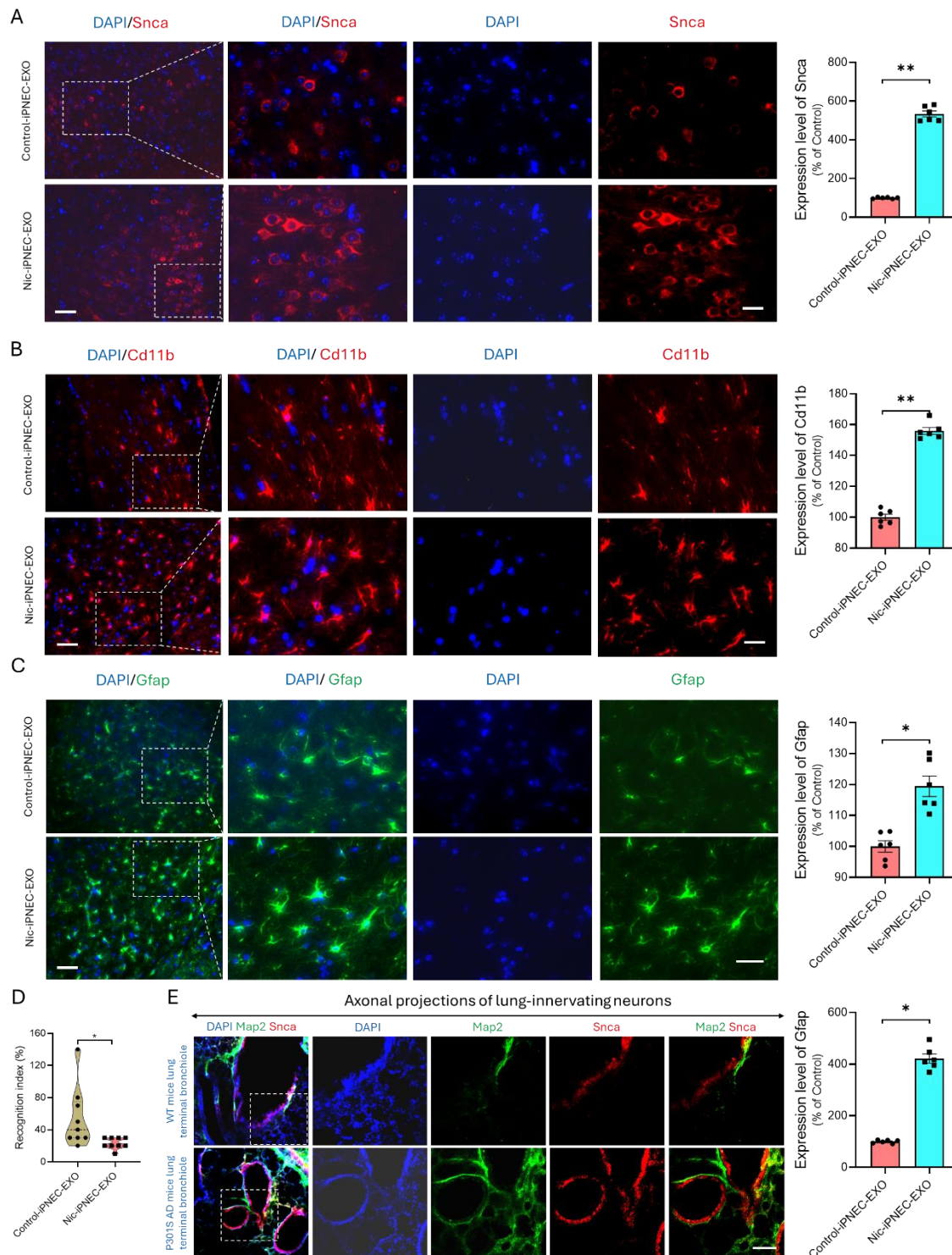
Supplementary Fig. S9. Detection of transferrin in the exosomes from control- and nicotine treated- iPNECs. Representative (**A**, **B**) immunogold-EM micrographs and (**C**) quantitative box plot showing the enhanced level of transferrin in exosomes from nicotine treated iPNECs as compared to the vehicle treated control group. Data were presented as mean \pm S.E.M. (N = 3 biological replicates; n = 6–10 vesicles quantified per replicate). Significance level: **P<0.01; Control vs. Nicotine group.



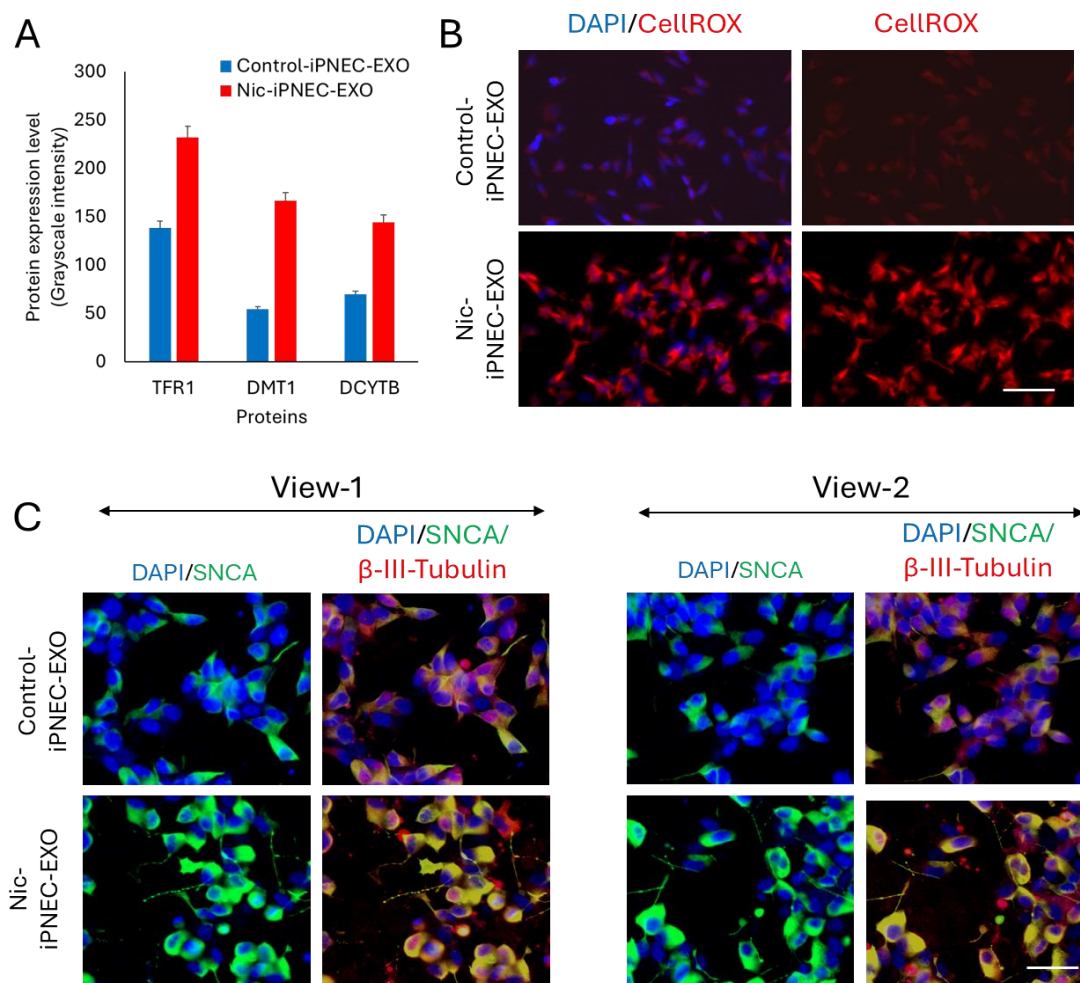
Supplementary Fig. S10. The effect of nicotine on the cognitive and motor behaviors of mice. (A) Representative images of track of mice in the novel object recognition test, and (B) a quantitative bar graph showing the decrease in percentage of recognition index, when the mice are administered with nicotine, compared to the vehicle treated control. (C) Experimental design of the Barnes maze and Damsel-in-Distress Paradigms, and quantitative bar graphs showing (D) the increase in latency time, and (E) the number of nose poke errors by the mice, administered with nicotine compared to the vehicle treated control. (F) A representative figure depicting the mice while being examined with mesh test (refer to the separate Supplementary Video S1), and (G) the quantitative bar graph showing the decrease in time required for the latency to fall by mice, administered with nicotine compared to the vehicle treated control. (H, I) Representative images of (H) track of mice in the open field test, and (I) a quantitative bar graph showing the enhanced time spent by mice in the center, when the mice are administered with nicotine, compared to the vehicle treated control. A total of six C57BL/6 mice were used per group (N=6). Data were presented as mean \pm S.E.M. Significance level: *P<0.05, **P<0.01, ns=not significant; Control vs. Nicotine groups.



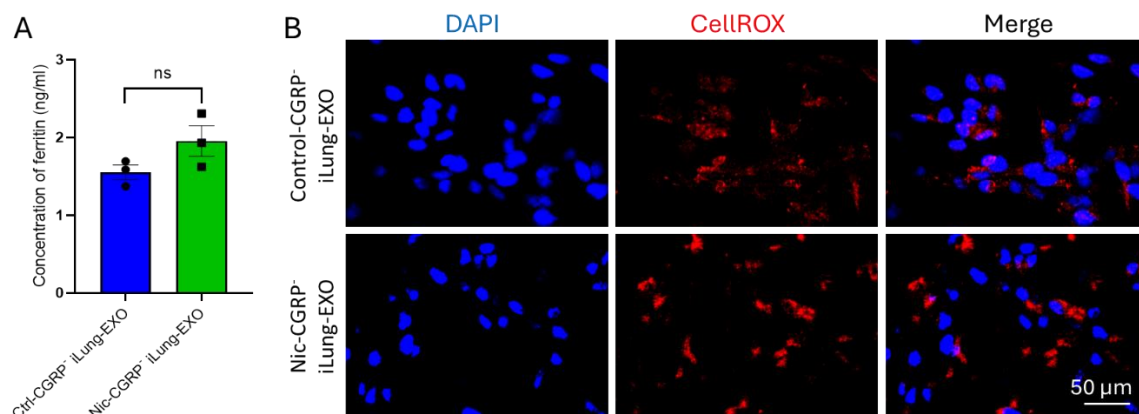
Supplementary Fig. S11. Alpha-synuclein is augmented in PNEC innervating-neurons in *in vitro*, human and mouse lungs. (A, B) Representative immunofluorescence staining and bar graph showing the expression of CGRP, P2Y1, and SNCA in the lung tissue sample of (A) non-smoking and (B) smoking human. **(C, D)** Representative immunofluorescence staining and bar graph showing the expression of Cgrp, P2y1, and Snca in the lung tissue sample of (C) control- and (D) nicotine treated- mouse. (Scale bar: 20 μ m).



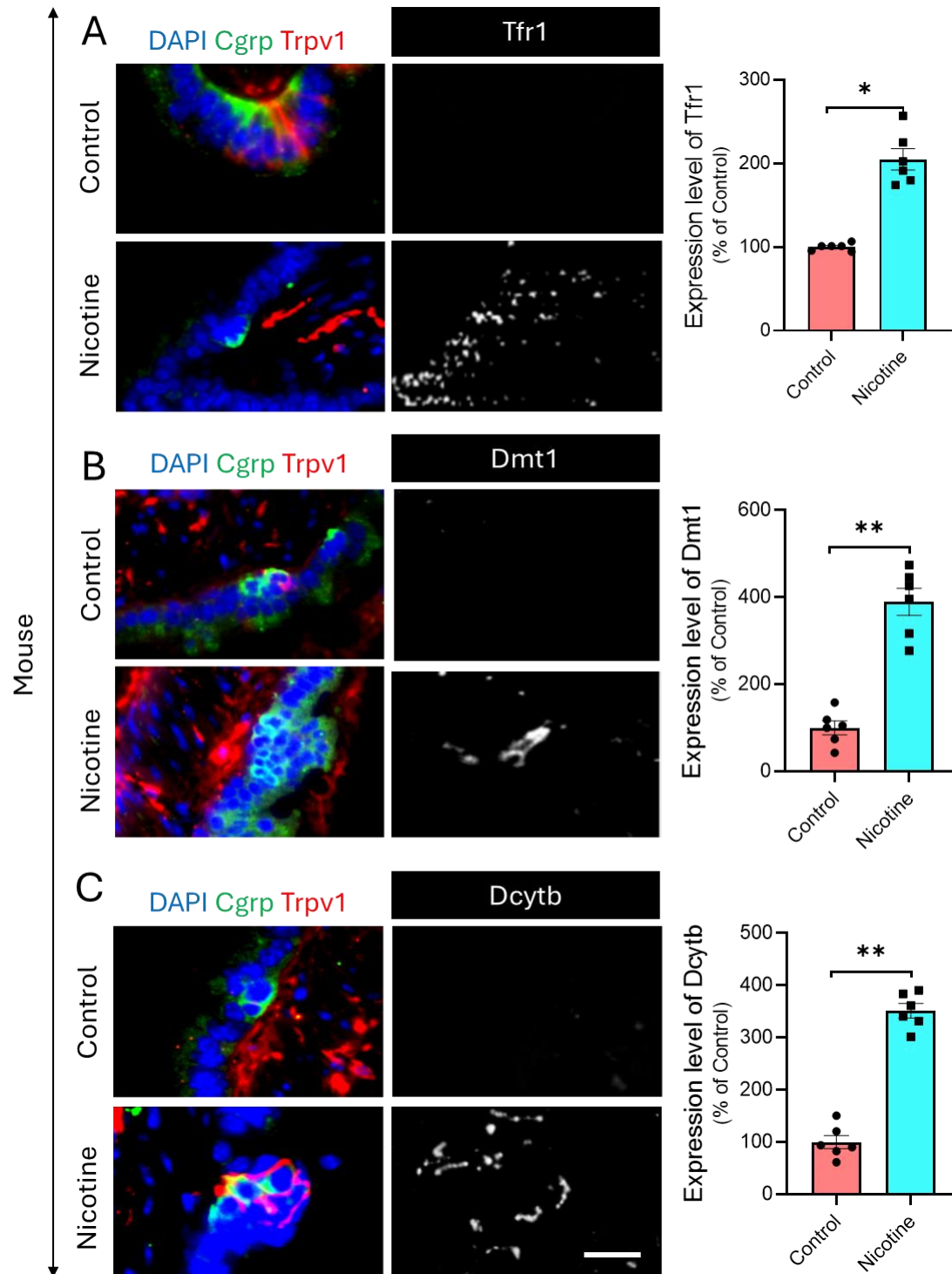
Supplementary Fig. S12. Effect of nicotine-iPNEC-EXO on the brain cells induced neuroinflammation-associated and vulnerability-related changes, and enhanced expression of SNCA in axonal neurons in lung of AD mice. Representative immunofluorescence staining images and quantitative bar graph of (A) Snca/DAPI, (B) Cd11b/DAPI, and (C) Gfap/DAPI in brain tissues of control- and nicotine- PNEC-EXO treated mice (Scale bar: 50 μ m). (D) Effect of control- and nicotine- iPNEC-EXO on the cognitive ability of mice, as determined by the novel object recognition test (Statistically analyzed by student t-test; * $P < 0.05$). (E) Representative immunofluorescence staining images and quantitative bar graph of depicting the enhanced Snca expression in axonal projections of lung innervating neurons, near terminal bronchiole (Scale bar: 100 μ m). Data were presented as mean \pm S.E.M. (N=6). Significance level: ** $P < 0.01$; Control-iPNEC-EXO vs. Nic-iPNEC-EXO.



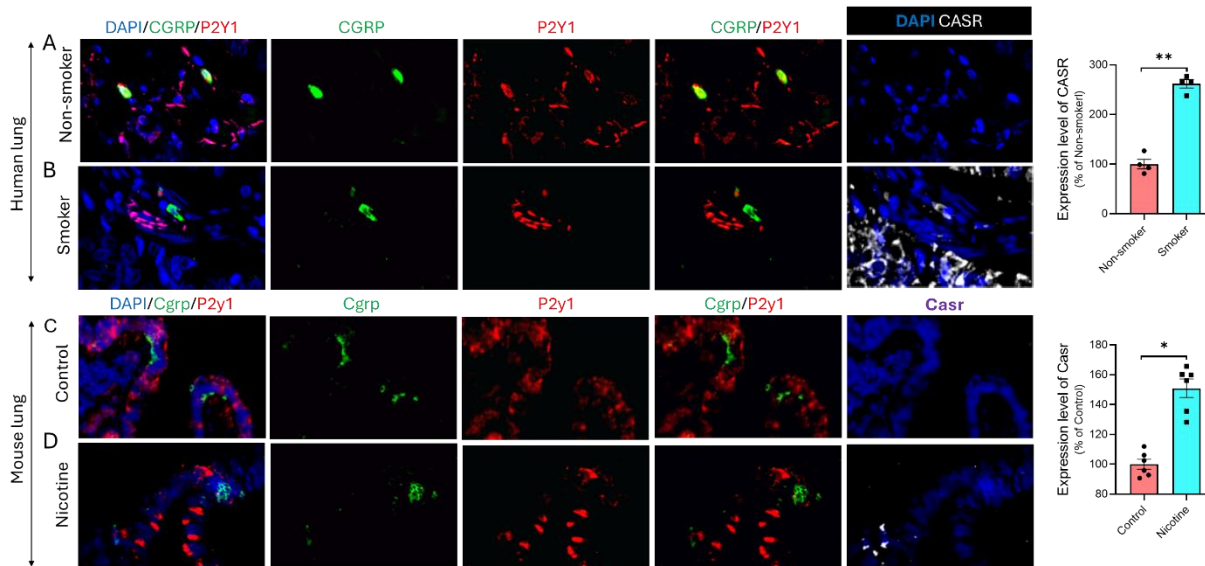
Supplementary Fig. S13. Effect of Nic-iPNEC-EXO on neuronal cells. (A) Expression levels of TFR1, DMT1, DCYTB in HD10.6 neuronal cells treated with control-iPNEC-EXO and Nic-iPNEC-EXO. (B, C) Additional views of immunofluorescence images shown in Fig. 4G,I,J showing the effect of control- or Nic- iPNEC-EXO on oxidative stress (scale bar = 50 μ m) and SNCA (scale bar = 20 μ m) in neuronal cells.



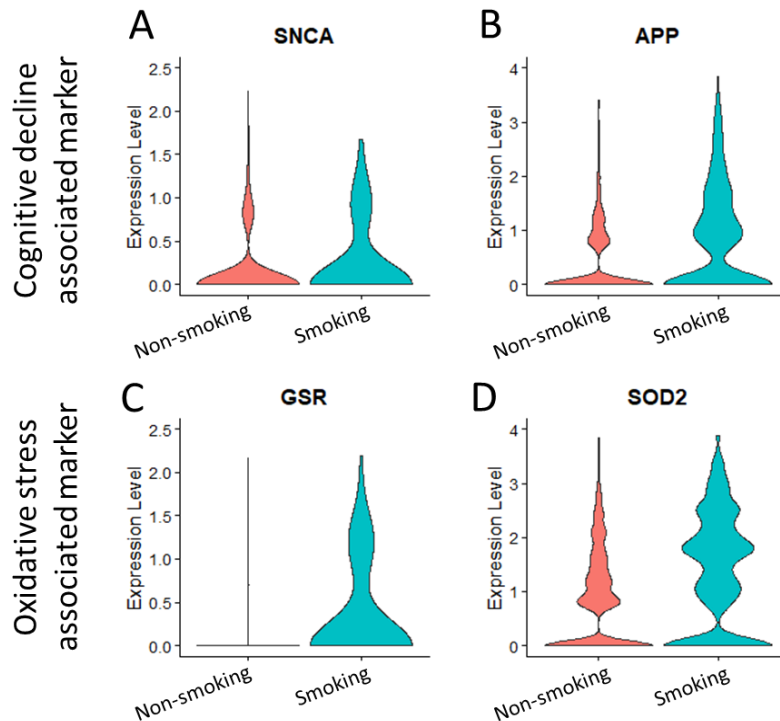
Supplementary Fig. S14. Effect of control and nicotine-exposed non-PNEC iLung cells-derived exosomes on neuronal cells. (A) Bar graph showing the effect of control- or nicotine- exposed non-PNEC iLung cells-derived exosomes on ferritin levels in neuronal cells. Data are presented as mean \pm S.E.M. (N=3). Significance level: * P <0.05, ns=not significant; Ctrl-CGRP⁺ iLung-EXO vs Nic-CGRP⁺ iLung-EXO. (B) Immunofluorescence staining images showing the effect of control- or nicotine- exposed non-PNEC iLung cells-derived exosomes on the oxidative stress in neuronal cells.



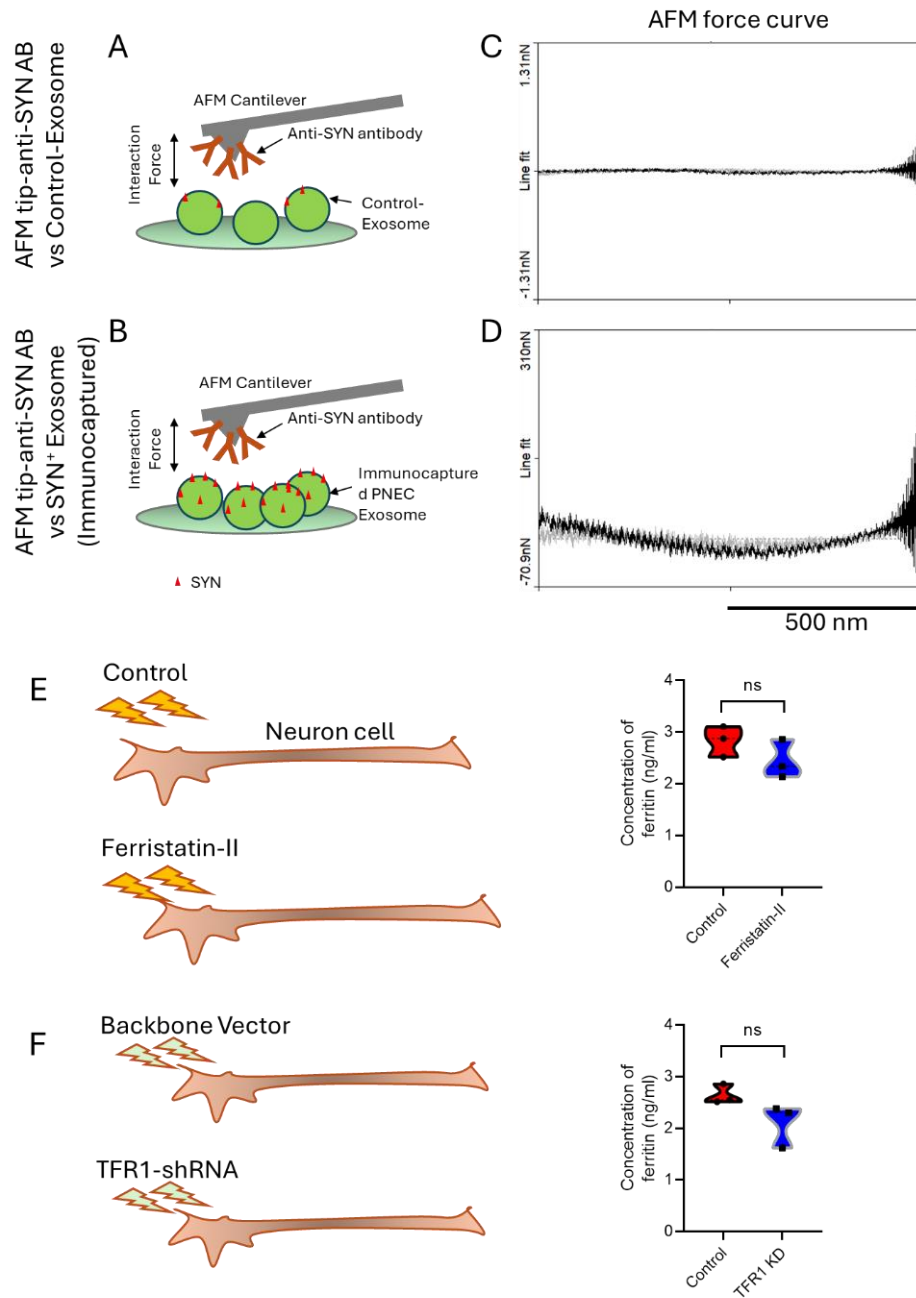
Supplementary Fig. S15. Effect of nicotine treatment on the iron homeostasis receptors on the PNEC innervating neurons in mice lungs. Representative immunofluorescence images showing the co-staining of proteins (A) DAPI, Cgrp, Trpv1, and Tfr1, (B) DAPI, Cgrp, Trpv1, and Dmt1, and (C) DAPI, Cgrp, Trpv1, and Dcytb in the lung tissue of WT control vs nicotine injected mice. (Scale bar: 20 μ m). Data were presented as mean \pm S.E.M. (N=6). Significance level: *P<0.05, **P<0.01, ns=not significant; Control vs Nicotine.



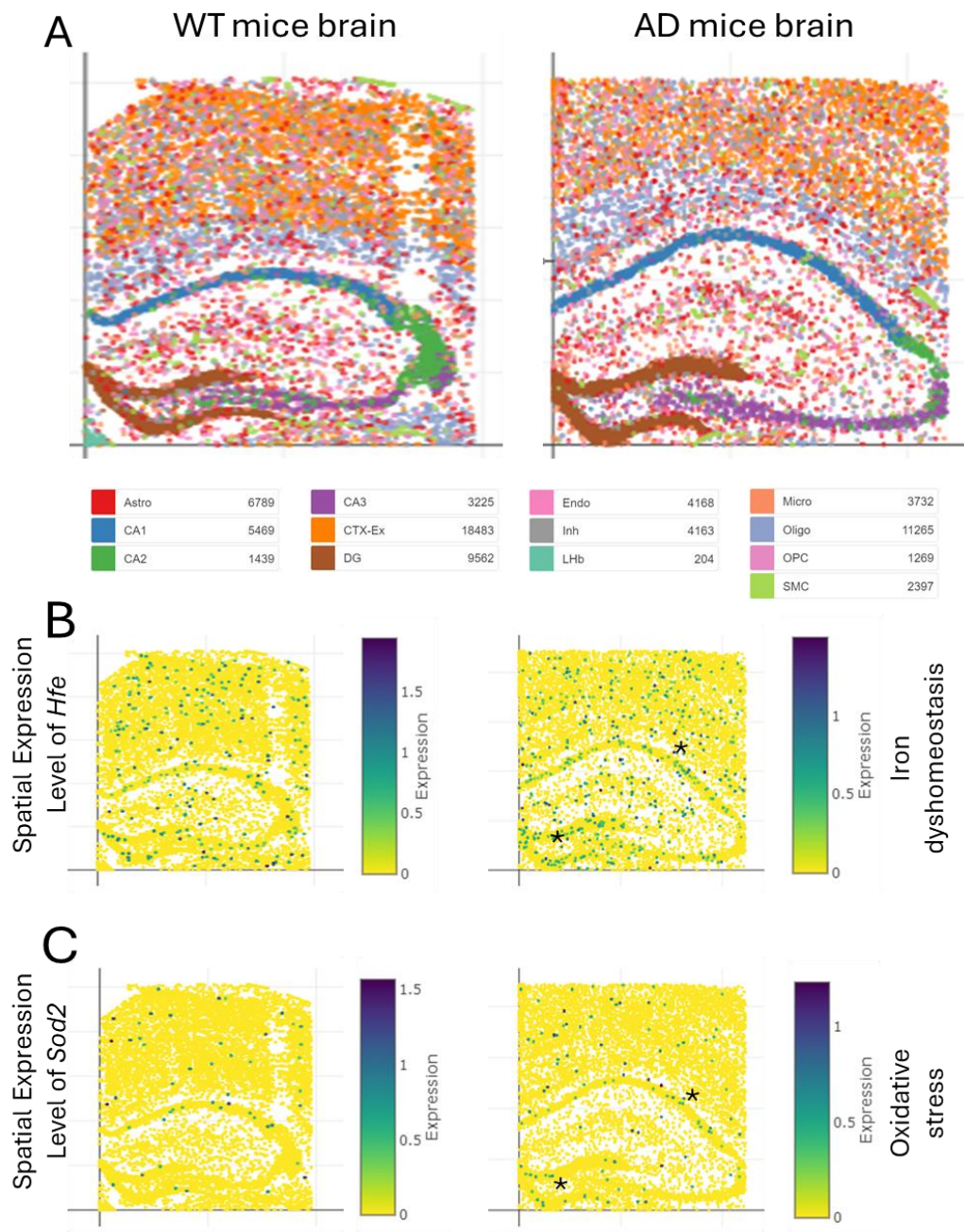
Supplementary Fig. S16. Calcium signaling is augmented in neuro-innervated PNECs in human and mouse lungs. (A, B) Representative immunofluorescence staining of CGRP, P2Y1, and CASR in the lung tissue sample of (A) non-smoking and (B) smoking human. (C, D) Representative immunofluorescence staining of Cgrp, P2y1, and Casr in the lung tissue sample of (C) control- and (D) nicotine treated- mouse. (Scale bar: 20 μ m). Data were presented as mean \pm S.E.M. (N=4 for A, B; N=6 for C, D). Significance level: *P<0.05, **P<0.01, ns=not significant; Non-smoker vs Smoker, Control vs Nicotine.



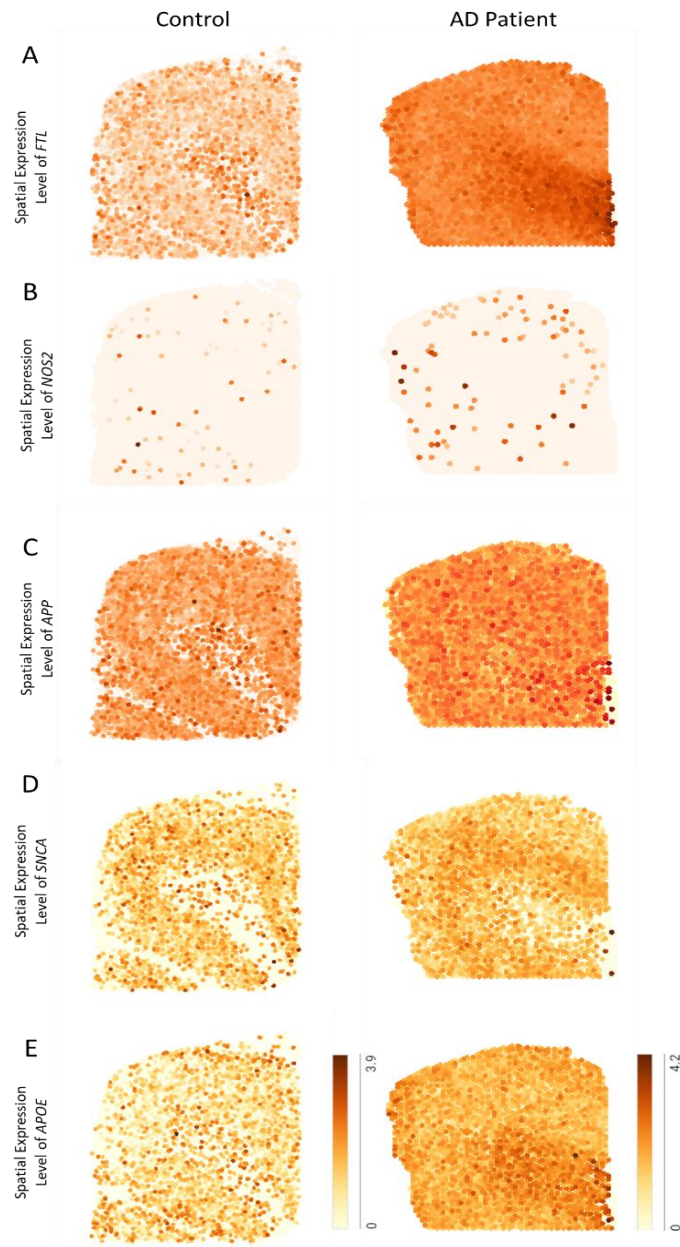
Supplementary Fig. S17. Effect of smoking on the cognition, and oxidative stress markers in neuronal cell population, detected by scRNA-seq of human lung. (A, B) Representative violin plots showing the expression of cognitive markers, (A) *SNCA* and (B) *APP* in *P2RY1*⁺ cell population from lungs of non-smoking and smoking humans. (C, D) Representative violin plots showing the expression of oxidative stress markers, (C) *GSR* and (D) *SOD2* in *P2RY1*⁺ cell population from lungs of non-smoking and smoking humans. (Total number of cells for: *P2RY1*_{non-smoking} = 908; *P2RY1*_{smoking} = 194). The scRNA-seq data used here for analysis was obtained from GEO: GSE122960 portal (Accession no.: GSE122960).



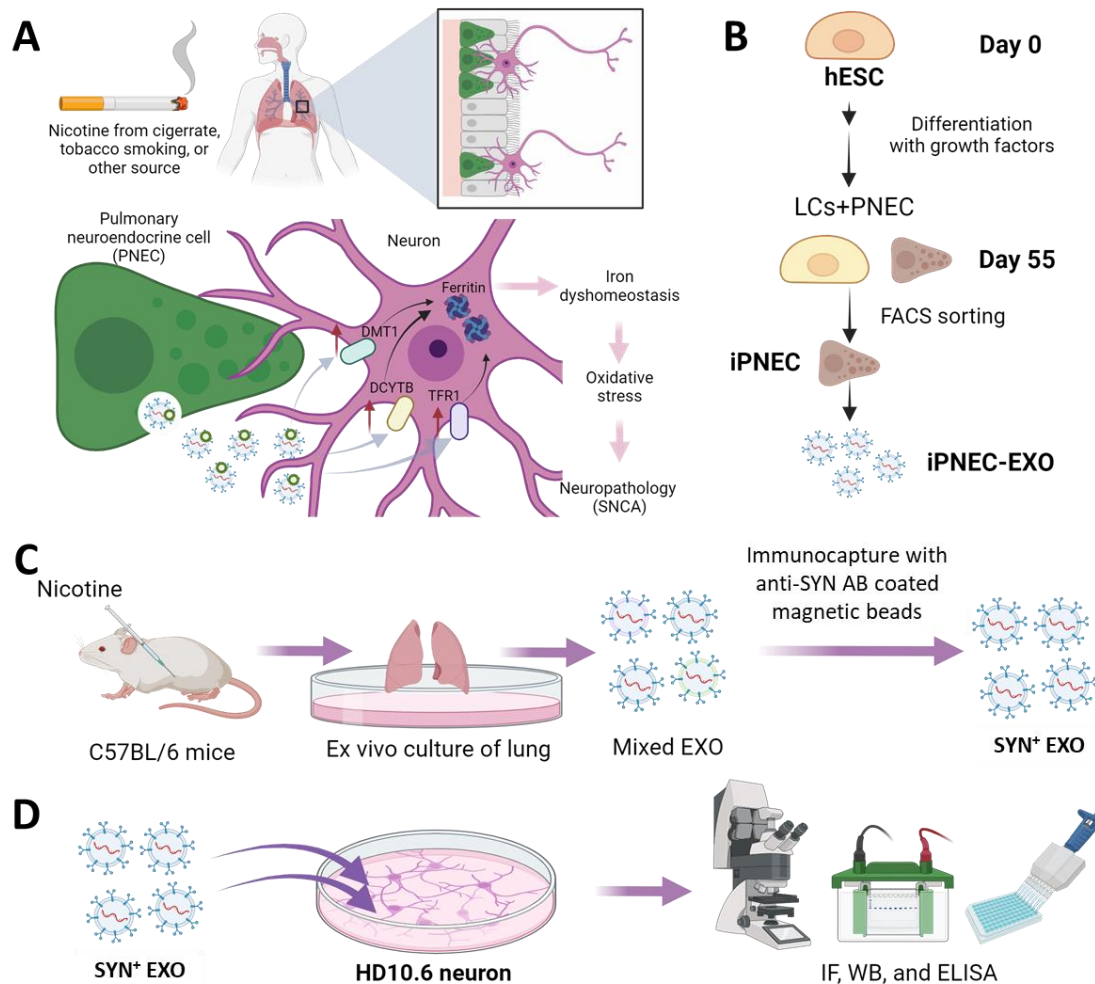
Supplementary Fig. S18. AFM based validation of immunocapture of SYN positive exosomes. (A, B) Representative diagram showing the AFM set-up equipped with cantilever functionalized with anti-SYN antibody (detail mention in method section) and exosome (without and with immunocaptured) samples immobilized on the mica-based sample disc, and (C, D) the corresponding AFM force curves. (E, F) Violin plots showing the effect of Ferristatin-II and TFR1 KD on the concentration of ferritin in neuronal cells. Data were presented as mean \pm S.E.M. (N=3). Significance level: *P<0.05, **P<0.01, ns=not significant; Control vs Ferristatin-II, Control vs TFR1 KD.



Supplementary Fig. S19. Evaluation of iron dyshomeostasis, oxidative stress and neurodegenerative markers in the brain of control and Alzheimer's disease (AD) mice. (A) Spatial expression showing the distribution of different cell types in control and AD mice's brain. The figures presented here are based on the analysis of the STARmap PLUS sequencing data (Single Cell Portal of Broad Institute, Study# SCP1375) and Zenodo (DOI: 10.5281/zenodo.7332091)(54). **(B, C)** Spatial expression analysis showing the augmented level of genes associated with (B) iron dyshomeostasis and (C) oxidative stress markers in AD patients' brain tissue compared to the control.

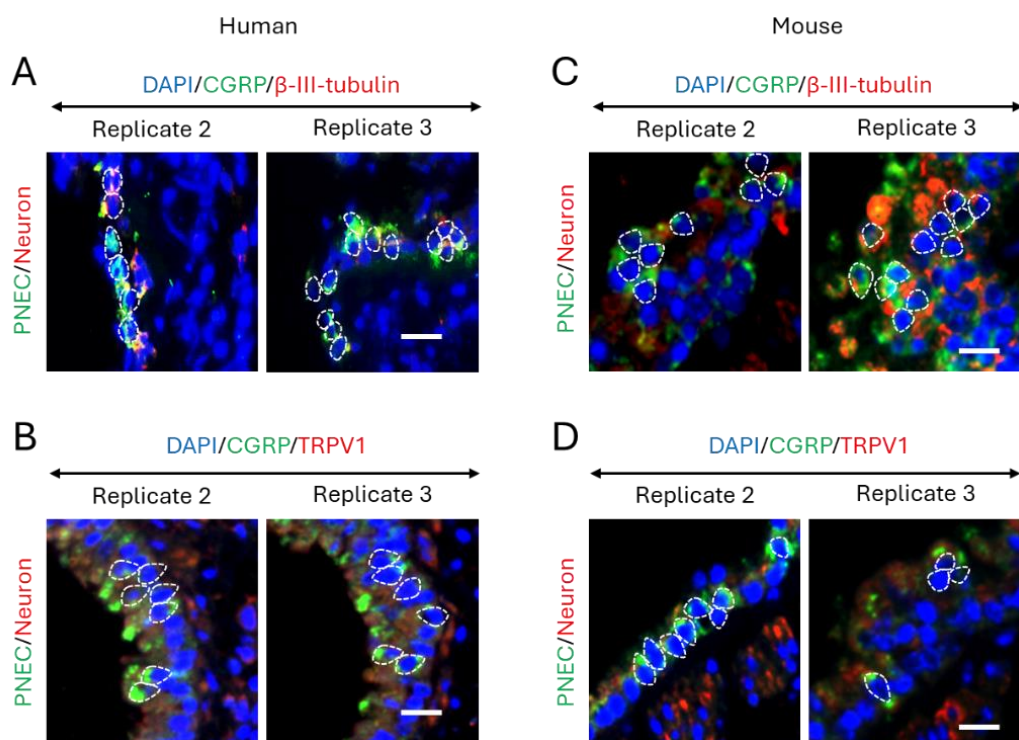


Supplementary Fig. S20. Evaluation of iron dyshomeostasis, oxidative stress and neurodegenerative markers in the brain of control and Alzheimer's disease patient. Spatial expression showing the enhanced expression and distribution of **(A)** *FTL* (depicting iron dyshomeostasis), **(B)** *NOS2* (depicting oxidative stress), and **(C-E)** *APP*, *SNCA*, and *APOE* in AD patient's brain as compared to that in control group, as determined by the STOmics analysis of the brain tissue of control (Dataset ID: STDS0000242; DOI: 10.1101/2024.01.31.576150) and AD patient (Dataset ID: STDS0000188; DOI: 10.1186/s40478-022-01494-6).

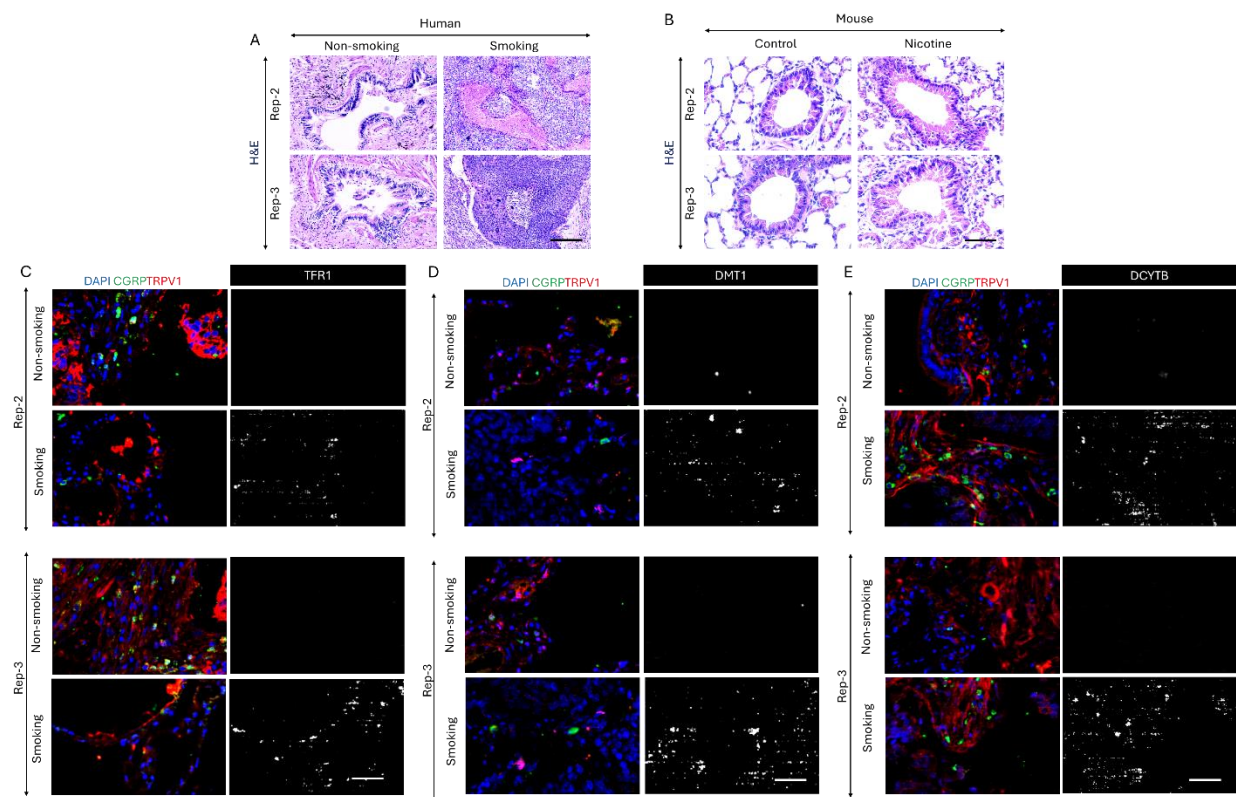


Supplementary Fig. S21. Sero transferrin enriched exosomes from PNEC perturbs the iron homeostasis and augment oxidative stress in neuronal cells. (A) Representative diagram showing the potential role of sero transferrin carried by PNEC-derived exosomes towards iron homeostatic imbalance in neuronal cells in the lung exposed to nicotine, a major constituent of cigarette or tobacco smoking. Briefly, nicotine can induce the increased release of PNEC-derived exosomes, which carry sero transferrin. The levels of TFR1, DMT1, and DCYTB are enhanced on the membrane of neuronal cells, facilitating the intracellular transport of iron, causing the enhanced accumulation of ferritin in neuronal cells, leading to oxidative stress. (B) Representative flow diagram showing the differentiation of hESC into a lung culture with PNEC, which was used for sorting out CGRP⁺ cells, depicting PNEC population (induced PNEC; iPNEC), followed by the isolation of exosomes (iPNEC-EXO). (C) Representative flow diagram showing the isolation of PNEC-EXO from the control- or nicotine treated- C57BL/6 mice's lung (cultured *ex vivo*) via anti-SYN antibody coated magnetic beads. (D) PNEC-EXO was incubated with HD10.6 neuronal cells for examining the effect on iron homeostasis and oxidative stress in neuronal cells.

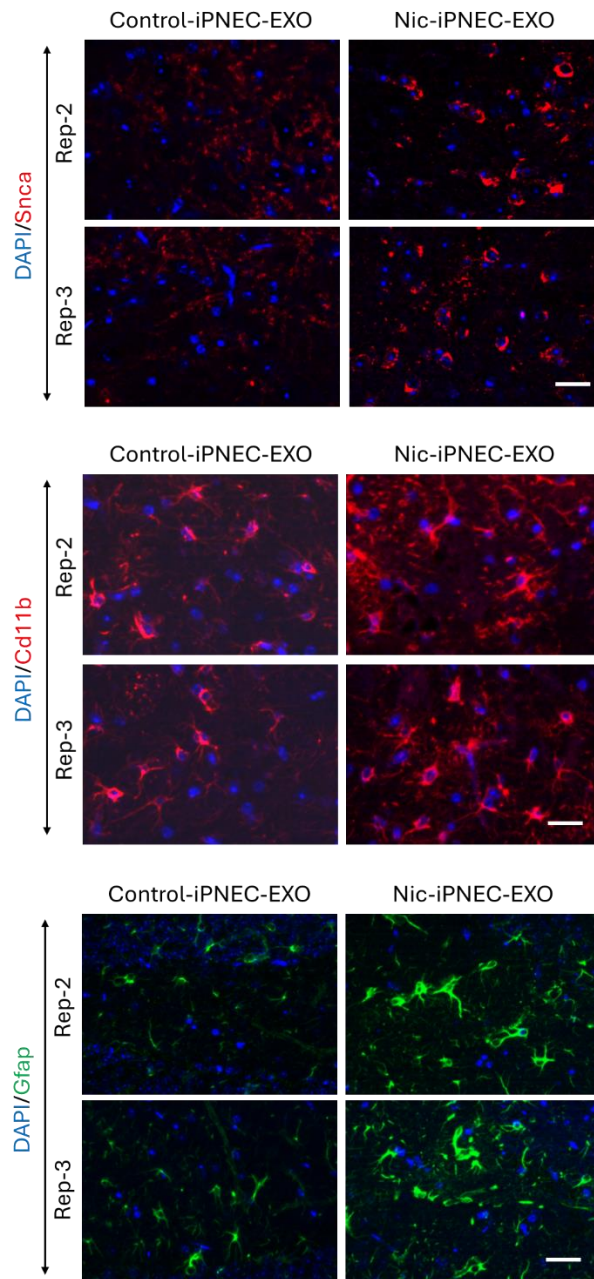
Additional Supporting Dataset



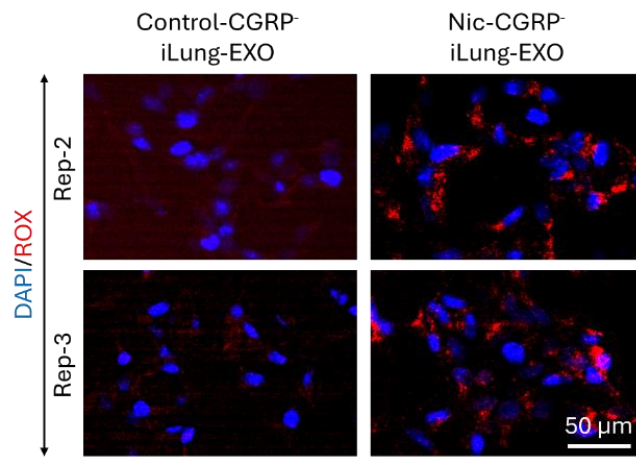
Supplementary Fig. S22. PNECs interact with neurons in lung. Additional immunofluorescence staining images support Figure 1A-D. Dashed outlines indicate representative PNECs scored towards interacting with neurons, illustrating the criteria used for manual scoring. Scale bar: 20 μ m.



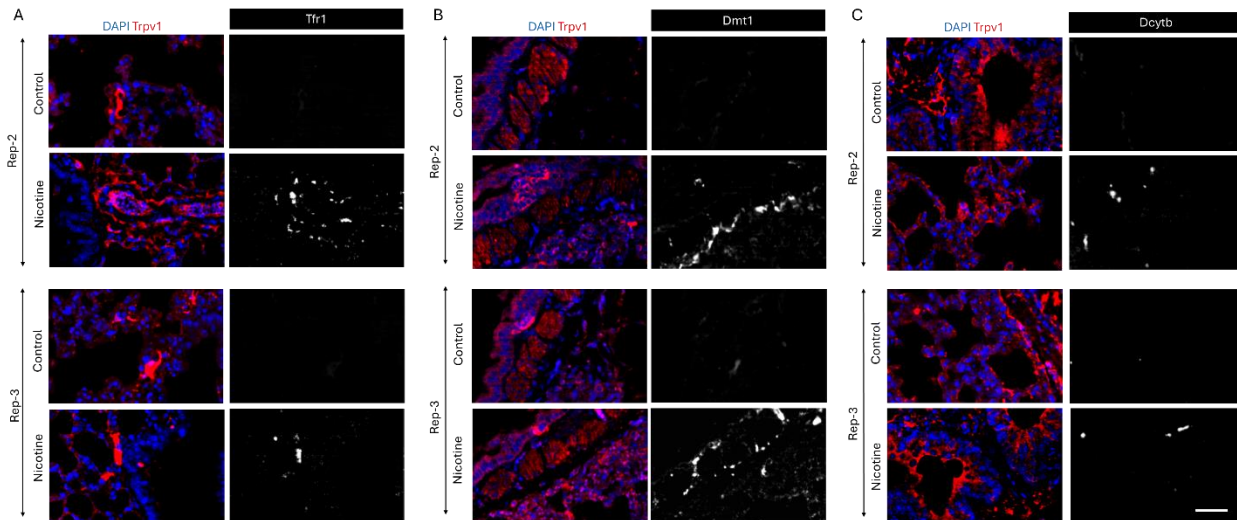
Supplementary Fig. S23. Additional H&E and immunofluorescence staining images supporting Figure 5F-H. (Scale bar: 50 μ m)



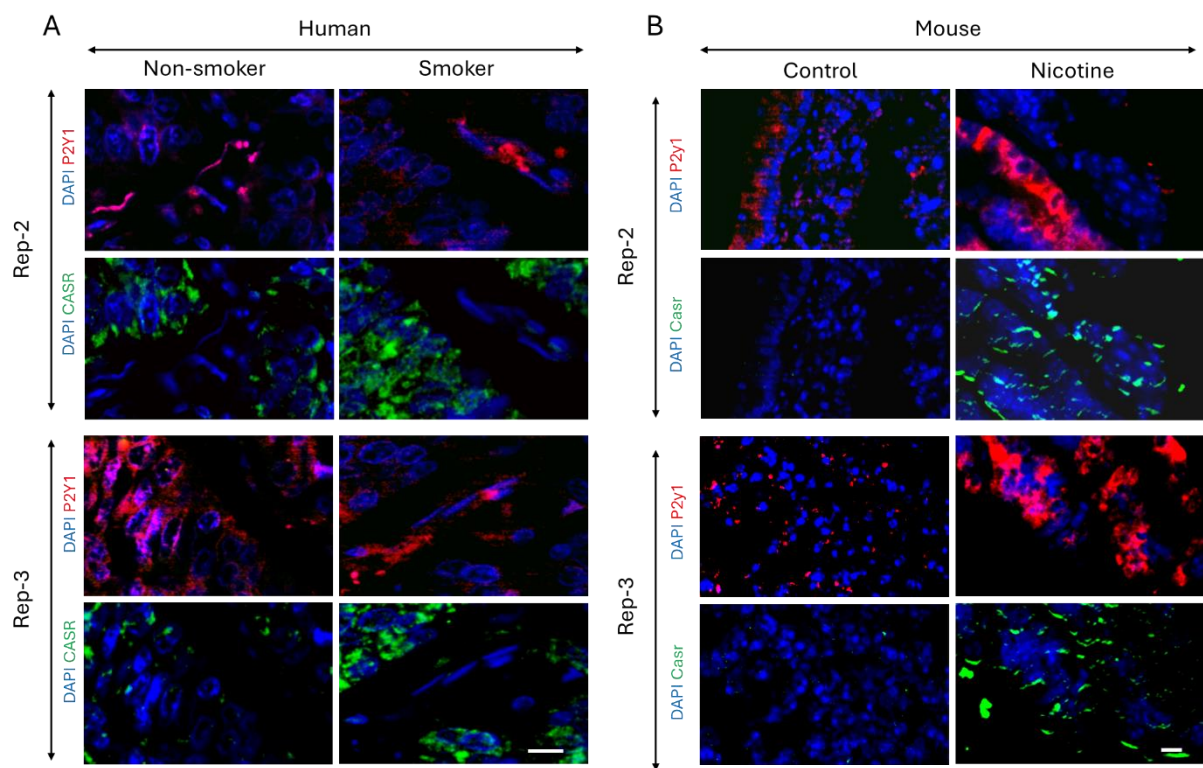
Supplementary Fig. S24. Effect of nicotine-iPNEC-EXO on the neuron and glia cells in mouse brain. Additional immunofluorescence staining images supporting Supplementary Figure S12. (Scale bar: 50 μ m)



Supplementary Fig. S25. Effect of nicotine exposed non-PNEC iLung cells-derived exosomes on neuronal cells *in vitro*. Additional immunofluorescence staining images supporting Supplementary Figure S14.



Supplementary Fig. S26. Additional immunofluorescence staining images supporting Supplementary Figure S15. (Scale bar: 20 μ m)



Supplementary Fig. S27. Additional immunofluorescence staining images supporting Supplementary Figure S16. (Scale bar: 20 μ m)

Supplementary Table S1. Information about human lung tissue samples from control, smoking, and AD groups. Refer to the excel file (Human patients' details_control_smoking_AD lung.xlsx)

Supplementary Table S2. List of antibodies and their relevant information.

Antibodies	Company	Catalogue	RRID	Dilution in IHC	Dilution in WB	Dilution in AFM	Dilution in immunogold-EM
Anti-CGRP polyclonal antibody	Invitrogen	PA1-85250	AB_2259435	1:100			
Anti-ASCL1 monoclonal antibody	Santa Cruz	sc374104	AB_10918561	1:100			
Anti-NKX2.1	Seven Hills Bioreagents	WRAB-1231	AB_2832953	1:100			
Anti-SOX2 antibody	Abcam	ab97959	AB_2341193	1:100			
Anti-TF	Abcam	Ab824	AB_306385	1:100			1:50
Anti-TFR1	Abcam	Ab84036	AB_10673794	1:100	1:1000		
Anti-DMT1	Abcam	ab55735	AB_2239227	1:100	1:1000		
Anti-DCYTB	Abcam	ab66048	Not available	1:100	1:1000		
Anti-CD63	Abcam	ab1318	AB_2076626	1:100			1:50
Anti-TRPV1	Abcam	ab6166	Not available	1:100			
Anti- β -III-Tubulin	Invitrogen	MA1-118	AB_2536829	1:100			
Anti-SYN	Abcam	ab526	AB_304526	1:100		1:50	
Anti-P2Y1	Abcam	ab168918	AB_90755	1:100			
Anti-FOXA2	Abcam	ab108422	AB_11157157	1:100			
Anti-SNCA	Invitrogen	PA5-85791	AB_2792927	1:100			
Anti-NeuN	Invitrogen	702022	AB_2633050	1:100			
Anti-CASR	Abcam	ab19347	AB_444867	1:100			
Anti- β -Actin	Santa Cruz	sc1616	AB_630836	1:100			
Goat anti-Rabbit IgG (H+L) Cross-Adsorbed Secondary Antibody, PE-Alexa Fluor 647	Invitrogen	A20991	AB_2535705	1:100			
Goat Anti-Rabbit IgG (H + L)-HRP Conjugate	BIO-RAD	170-6515	AB_11125142	1:5000	1:5000		
Goat Anti-Mouse IgG (H + L)-HRP Conjugate	BIO-RAD	170-6516	AB_2921252	1:5000	1:5000		
Anti-Rabbit Secondary gold nanoparticle (10 nm)	Abcam	Ab270555	Not available	1:50			

Supplementary Video S1. A video showing the performance of control- and nicotine treated- mice, depicting the motor strength during mesh test results shown in Supplementary Figure S10F, G.